Electrostatic Binding of Polyanions using Self-Assembled Multivalent (SAMul) Ligand Displays – Structure-Activity Effects on DNA/Heparin Binding

Loryn E. Fechner[a], Buthaina Albanyan[a], Vânia M. P. Vieira,[a] Erik Laurini[b], Paola Posocco[b], Sabrina Pricl[b,*] and David K Smith[a,*]

SUPPORTING INFORMATION

Contents

1. General Experimental Methods.

All compounds required in synthesis and analysis were purchased from standard commercial suppliers. Proton and carbon NMR spectra were recorded on a Jeol 400 spectrometer (^{1}H 400 MHz, ^{13}C 100 MHz). A Bruker 500 (^{1}H 500 MHz) was used for kinetics experiments. Samples were recorded as solutions in deuterated NMR solvents as stated and chemical shifts (δ) are quoted in parts per million. Coupling constant values (J) are given in Hz. The level of assignment of ^{1}H NMR spectra was achieved using model compounds, literature data and standard knowledge of ^{1}H NMR. DEPT experiments were used to assist in the assignment of ^{13}C NMR spectra. Positive and negative ion electrospray mass spectra were recorded on a Bruker Daltonics MicroTOF mass spectrometer. IR spectra were recorded on a PerkinElmer Spectrum Two FT-IR spectrometer. Melting points were measured on a Stuart SMP3 melting point apparatus and are uncorrected. UV-vis absorbance was measured on a Shimadzu UV-2401 PC spectrophotometer. Fluorescence was measured on a Hitachi F-4500 spectrofluorimeter.

2. Synthesis and Characterisation of Compounds

Boc-Protected Amine Synthesis. Diaminopropane (DAP) and *N*,*N*-di-(3-aminopropyl)-*N*-methylamine (DAPMA) were mono-Boc protected using methods adapted from those in the literature for mono-amine protection. Spermine was tri-Boc protected using a one-pot procedure originally reported by Blagborough and co-workers.[1] Spermidine could not be trivially Boc protected owing to its non-symmetric nature, and as such was constructed in protected form using a standard approach of cyanoethylation of mono-Boc-protected diaminobutane using Michael addition chemistry followed by Boc protection of the secondary amine and final reduction of the nitrile using lithium aluminium hydride.[2] All Boc-protected amines had spectroscopic data fully consistent with their identities.

General Procedure for Coupling Bo-Protected Amines with Palmitic Acid. Palmitic acid (1.0 eq.) was dissolved in DCM (65 ml) and TBTU (1.0 eq.) and NEt_3 (approx. 5 ml) were added. The mixture was stirred for 5 minutes, then the protected polyamine (1.0 eq.) was dissolved in DCM and added to the mixture. The solution was left stirring overnight. The

solvent was evaporated *in vacuo*. The purification of the product was achieved by column chromatography as detailed for each compound.

Boc-Protected C_{16}-DAP. Quantities: Palmitic acid (1.00 g, 3.9 mmol), mono-Boc-DAP (683 mg, 3.9 mmol), TBTU (1.25 g, 3.9 mmol). The product was purified by column chromatography (DCM to DCM/MeOH (9:1)). The product was isolated as a white powder 1.50 g, 93%). R_f (DCM/MeOH, 9:1) 0.43. ^{1}H NMR (400 MHz, $CDCl_3$): δ = 6.22 (br s, N*H*, 1H), 4.93 (br s, N*H*Boc, 1H), 3.29 (td, CH_2NHCO, J = 6.2, 6.4 Hz, 2H), 3.16 (td, CH_2N(CH_3), J = 6.0, 5.6 Hz, 2H), 2.18 (t,CH_2CONH, J = 7.6 Hz, 2H), 1.60 (m, C$H_2$$CH_2$CONH + CH_2C$H_2$$CH_2$, 4H), 1.43 (s, C(C$H_3$)$_3$, 9H), 1.32-1.24 (m, CH_3(CH_2)$_{12}$$CH_2$, 24H), 0.87 (t, C$H_3$$CH_2$, J = 7.0 Hz, 3H). ^{13}C NMR (100 MHz, $CDCl_3$): δ = 173.85 (*C*=O), 79.52 (*C*(CH_3)$_3$), 37.02 (*C*H_2NHCO), 32.07 (NH*C*$H_2$$CH_2$*C*$H_2$NH), 30.44, 29.83, 29.8,29.65, 29.51, 29.45, 28.53, 25.95 (NH*C*H_2*C*$H_2$$CH_2$NH + (*C*$H_2$)$_{12}$CO), 22.84 (*C*$H_2$$CH_3$), 14.28 (*C*$H_3$$CH_2$). IR: 3360.3*m* , 3310.0*m*, 2918.3*s*, 2851.3*s*, 1685.8*s*, 1639.0*s*, 1538.4*m*, 1468.1*w*, 1444.7*w*, 1391.0*w*, 1364.3*w*, 1280.6*m*, 1253.8*w*, 1173.4*m*, 1133.2*w*, 721.2*w*. ESI-TOF-MS calc for $C_{24}H_{50}N_2O_3$: 413.3738; found: 413.3719 (33%, $[M+H]^+$), 435.3571 (100%, $[M+Na]^+$).

Boc-Protected C_{16}-DAPMA. Quantities: Palmitic acid (1.00 g, 3.9 mmol), mono-Boc-DAPMA **(2)** (950 mg, 3.9 mmol), TBTU (1.25 g, 3,9 mmol). After evaporation of solvent the product was dissolved again in EtOAc (50 ml) and washed two times with sat. $NaHSO_4$ (15 ml), two times with sat. $NaHCO_3$ (15 ml), three times with H_2O (15 ml) and once with sat. NaCl (15 ml). After GPC (DCM), the product was obtained as white solid (1.70 g, 3.5 mmol, 90 %). R_f (DCM:MeOH:NEt_3, 90:10:0.1) 0.08. ^{1}H NMR (400 MHz, $CDCl_3$): δ = 6.82 (br s, N*H*, 1H), 5.1 (br s, N*H*Boc, 1H), 3.34 (td, CH_2NHCO, J = 5.9, 6.0 Hz, 2H), 3.20 (td, CH_2NHBoc, J = 5.6, 5.5 Hz, 2H), 2.73 (br , CH_2N(CH_3), 4H), 2.47 (s, N(CH_3), 3H), 2.18 (t, J = 7.2 Hz, CH_2CONH, 2H), 1.86 (m, C$H_2$$CH_2$N($CH_3$), 4H), 1.60 (t, C$H_2$$CH_2$CONH, J = 7.2 Hz, 2H), 1.43 (s, C(CH_3)$_3$, 9H), 1.32-1.24 (m, CH_3(CH_2)$_{12}$$CH_2$, 24H), 0.87 (t, C$H_3$$CH_2$, J = 6.8 Hz, 3H). ^{13}C NMR (100 MHz, $CDCl_3$): δ = 173.99 (*C*=O), 156.31 (*C*=*O*Boc), 77.50, 77.10, 76.71, 36.83 (*C*H_2NHCO), 31.87 (*C*$H_2$$CH_2$$CH_3$), 29.60 (*C*$H_2$$CH_2$$CH_2$), 29.39 (*C*$H_2$$CH_2$$CH_2$CO), 28.24 (C(*C*$H_3$)$_3$), 25.84 (*C*$H_2$$CH_2$CO), 22.57 (*C*$H_2$$CH_3$), 13.98 (*C*$H_3$$CH_2$). ESI-TOF-MS calc. for $C_{28}H_{58}N_3O_3$: 484.4473, found: *m/z* (%): 484.4474 (100%, $[M+H]^+$).

Boc-Protected C_{16}-Spermidine. Quantities: Palmitic acid (0.472 g, 1.84 mmol, 1.04 eq.), N^1,N^5-Bis-Boc-spermidine (0.61 g, 1.76 mmol), TBTU (0.585 g, 1.82 mmol), NEt_3 (3.5 ml). After the solvent was evaporated some of the crude product (700 mg from 2.10 g) was purified, first by GPC in DCM and second by column chromatography (SiO_2 in Hex/EtOAc 1:1). The product was obtained as a white powder (258 mg, purified material, equivalent to 76% if all was purified). R_f (Hex:EtOAc, 1:1) 0.23. ^{1}H NMR (400 MHz, $CDCl_3$): δ = 6.72 (br s, N*H*, 1H), 4.55 (br s, N*H*Boc, 1H), 3.27-3.13 (m, CH_2NHCO, 8H), 2.17 (t, J = 7.6 Hz, CH_2CONH, 2H), 1.68-1.52 (m, CH_2CH$_2$NBoc + (CH_2)$_2$CH$_2$NHBoc + CH_2CH$_2$CONH, 8H), 1.45 + 1.43 (2 s, C(CH_3)$_3$, 18H), 1.32-1.24 (m, CH$_3$(CH_2)$_{12}$CH$_2$, 24H), 0.87 (t, CH_3CH$_2$, J = 6.8 Hz, 3H). ^{13}C NMR (100 MHz, $CDCl_3$): δ = 172.11 (*C*=O), 156.14 (*C*=*O*Boc), 79.88 (*C*(CH$_3$)$_3$), 46.65 ((*C*H$_2$)$_2$NCO), 37.15 (*C*H$_2$NHCO), 32.07 (*C*H$_2$NHCOBoc), 29.83, 29.80, 29.66, 29.53, 29.50, 29.47, 28.55 (C(*C*H$_3$)$_3$), 27.61, 25.96 (*C*H$_2$CH$_2$CO), 22.83 (*C*H$_2$CH$_3$), 14.27 (*C*H$_3$CH$_2$). ESI-TOF-MS calc. for $C_{33}H_{66}N_3O_5$: 584.4997; found: 584.4997 (24%, $[M+H]^+$), 606.4829 (100%, $[M+Na]^+$).

Boc-Protected C_{16}-Spermine. Quantities: Palmitic acid (0.76 g, 2.98 mmol) in 65 ml DCM, tri-Boc-spermidine (1.50 g, 2.98 mmol), TBTU (0.95 g, 2.98 mmol). After the solvent was evaporated product was purified first by silica column in DCM/MeOH (1:0 to 9:1). Two fractions were combined (2.5 g) and purified again by a second column in Hex/EtOAc 2:1. The product was obtained as a colourless oil (448 mg, 28 %). After 72 h some white crystals formed in the oil. R_f (Hex:EtOAc, 1:1) 0.22. ^{1}H NMR (400 MHz, $CDCl_3$): δ = 8.29 (br s, N*H*, 1H), 5.27 (br s, N*H*Boc, 1H), 3.13-3.25 (m, CH_2NHCO + CH_2NBoc + CH_2NHBoc, 12H), 2.17 (t, J = 7.6 Hz, CH_2CONH, 2H), 1.69-1.60 (m, CH_2CH$_2$NBoc + (CH_2)$_2$CH$_2$NHBoc, 8H), 1.45 (s, C(CH_3)$_3$, 27H), 1.32-1.24 (m, CH$_3$(CH_2)$_{12}$CH$_2$ +CH_2CH$_2$CONH, 26H), 0.87 (t, CH_3CH$_2$, J = 7.0 Hz, 3H). ESI-TOF-MS calc. for $C_{41}H_{81}N_4O_7$: 741.6100; found: 741.6095 (25%, $[M+H]^+$), 763.5915 (100%, $[M+Na]^+$).

General Procedure for Boc Deprotection. The Boc-protected precursor was dissolved in MeOH, and HCl gas was bubbled through the solution for approximately 15 seconds. The mixture was then stirred for at least 3 hours and the solvent removed *in vacuo* to yield the target compounds.

C_{16}-DAP. Boc-Protected C_{16}-DAP (1.3 g, 3.15 mmol) was reacted, and after drying in vacuum, the product was obtained as a white solid (1.1 g, quant.). ^{1}H NMR (400 MHz, CD_3OD): δ = 3.24 (t, *J* = 6.8 Hz, C*H*$_2$NHCO, 2H), 2.89 (t, C*H*$_2$NH$_2$, *J* = 7.2 Hz, 2H), 1.80 (app. quint., J = 7.0 Hz, C*H*$_2$CH$_2$NH$_2$, 2H), 1.57 (app. quint., J = 6.6 Hz, C*H*$_2$CH$_2$CONH, 2H), 1.25 (br s, (C*H*$_2$)$_{12}$, 24 H), 0.87 (t, C*H*$_3$CH$_2$, J = 7.0 Hz, 3H). ^{13}C NMR (100 MHz, CD_3OD): δ = 38.19 (*C*H$_2$NH$_2$), 36.96 (*C*H$_2$NHCO), 36.80 (*C*H$_2$CONH), 33.08 (*C*H$_2$CH$_2$NH$_2$), 30.79 (*C*H$_3$*C*H$_2$*C*H$_2$), 30.63, 30.48, 30.36 (C$_3$H$_7$(*C*H$_2$)$_{10}$), 28.84 ((*C*H$_2$)$_2$CH$_2$CH$_2$CONH), 27.00 (*C*H$_2$CH$_2$CONH), 23.74 (*C*H$_2$CH$_3$), 14.44 (*C*H$_3$) (C=O peak was not observed owing to low intensity spectrum). IR: 3287*m*, 2955*m*, 2918*s*, 2848*s*, 1642*s*, 1616*w*, 1555*m*, 1525*w*, 1468*w*, 1438*w*, 1267*w*, 1163*w*, 1009*w*, 721*w*. ESI-TOF-MS calc. for $C_{19}H_{41}N_2O$: 313.3213; found: 313.3215 (100%, $[M+H]^+$).

C_{16}-DAPMA. Boc-Protected DAPMA (1.79 g 3.70 mmol) was reacted, and after drying in vacuum, the product was obtained as slightly orange solid (1.70 g. quant.). ^{1}H-NMR (400 MHz, CD_3OD): δ = 3.05-3.29 (m, C*H*$_2$NH$_2$ + C*H*$_2$NHCO, 4H), 3.04 (t, C*H*$_2$N(CH$_3$), *J* = 7.4 Hz, 4H), 2.22 (t, C*H*$_2$CONH, *J* = 8.0 Hz, 2H), 2.12 (app. quint., *J* = 7.8 Hz, C*H*$_2$CH$_2$*N(CH$_3$)*), 2H), 1.95 (quint., *J* = 6.8 Hz, C*H*$_2$CH$_2$*NH$_2$*), 2H), 1.56 (app. quint., C*H*$_2$CH$_2$CONH, *J* = 6.0 Hz, 2H), 1.24-1.19 (m, CH$_3$(C*H*$_2$)$_{12}$, 24H), 0.86 (t, C*H*$_3$CH$_2$, *J* = 5.4 Hz, 3H). ^{13}C-NMR (100 MHz, CD_3OD): δ = 177.42 (*C*ONH), 55.24, 54.22 (*C*H$_2$N(CH$_3$)), 40.30 (N(*C*H$_3$)), 37.77 (*C*H$_2$CO), 37.16 (*C*H$_2$NHCO), 36.80 (*C*H$_2$NH$_2$), 32.99 (*C*H$_2$CH$_2$CH$_3$), 30.71 (*C*H$_2$CH$_2$CH$_2$), 30.39 (*C*H$_2$CH$_2$CH$_2$CO), 26.91 (*C*H$_2$CH$_2$NH), 25.48 (*C*H$_2$CH$_2$CO), 23.65 (*C*H$_2$CH$_2$NH$_2$), 23.43(*C*H$_2$CH$_3$), 14.37 (*C*H$_3$CH$_2$). IR: 3370*m*, 2955*m*, 2922*s*, 2851*s*, 2664*w*, 1642*m*, 1612*m*, 1542*m*, 1468*s*, 1378*m*, 1260*w*, 1234*w*, 1160*w*, 1070*w*, 738*s*. ESI-TOF-MS calc. for ($C_{23}H_{50}N_3O$): 384.3948; found: 384.3961 (100%, $[M+H]^+$).

C_{16}-Spermidine (C_{16}-SPD). Boc-Protected Spermidine (258 mg) was reacted, and after drying in vacuum, product was obtained salt as a white solid (209 mg, quant). ^{1}H NMR (400 MHz, CD_3OD): δ = 3.25 (t, *J* = 6.6 Hz, C*H*$_2$NHCO), 3.12-3.03 (m, C*H*$_2$NH + C*H*$_2$NH$_2$, 6H), 2.22 (t, *J* = 7.6 Hz, C*H*$_2$CONH, 2H), 1.92 (quint, *J* = 7.6 Hz, C*H*$_2$CH$_2$NHCO), 1.78 (app. quint, *J* = 4.0 Hz, C*H*$_2$CH$_2$NH$_2$ + C*H*$_2$CH$_2$CONH, 4H), 1.55 (br quint, C*H*$_2$CH$_2$CH$_2$NH$_2$, 2H), 1.24 (br s, CH$_3$(C*H*$_2$)$_{12}$CH$_2$, 24H), 0.84 (t, C*H*$_3$CH$_2$, *J* = 6.8 Hz, 3H). IR: 3308*m*, 2954*m*, 2916*s*, 2849*s*, 2788*m*, 2746*m*, 1644*s*, 1613*m*, 1543*s*, 1526*s*, 1464*s*, 1439*w*, 1360*m*, 1344*m*, 1269*m*, 1204, 1172*m*, 1090*m*, 1059*m*, 1015*m*, 757*m*, 728*m*, 680*m*, 600*w*, 550*m*, 458*w*. ESI-

TOF-MS calc. for $C_{23}H_{50}N_3O$: 384.3948; found: 384.3948 (100%, $[M+H]^+$). Solubility problems prevented the measurement of ^{13}C NMR.

C_{16}-Spermine (C_{16}-SPM). Boc-Protected Spermine (448 mg) was reacted, and after drying in vacuum, product was obtained as a white solid (323 mg, 97 %). ^1H NMR (400 MHz, $CDCl_3$): δ = 3.25 (t, *J* = 6.8 Hz, C*H*$_2$NHCO), 3.17-3.03 (m, C*H*$_2$NH + C*H*$_2$NH$_2$, 10H), 2.22 (t, *J* = 7.4 Hz, C*H*$_2$CONH, 2H), 2.08 (app. quint., *J* = 7.9 Hz, C*H*$_2$CH$_2$NH$_2$, 2H), 1.89 (approx. quint., *J* = 7.0 Hz, C*H*$_2$CH$_2$NHCO, 2H), 1.78 (m, CH$_2$(C*H*$_2$)$_2$CH$_2$, 4H), 1.55 (approx. quint, J = 6.0 Hz, C*H*$_2$CH$_2$CONH, 2H), 1.24 (s, CH$_3$(C*H*$_2$)$_{12}$CH$_2$, 24H), 0.84 (t, C*H*$_3$CH$_2$, *J* = 6.6 Hz, 3H). IR: 3317*m*, 2954*s*, 2918*s*, 2849*s*, 2782*s*, 2750*s*, 1703*s*, 1645*s*, 1531*s*, 1488*m*, 1464*s*, 1444*m*, 1411*w*, 1388*m*, 1349*m*, 1269*m*, 1250*m*, 1209*m*, 1182*s*, 1164*s*, 1087*w*, 1058*m*, 979*w*, 872*w*, 761*m*, 724*m*, 678*m*, 550*w*. ESI-TOF-MS calc. for $C_{26}H_{58}N_4O$: 441.4527; found: 441.4541 (100%, $[M+H]^+$). Solubility problems prevented the measurement of ^{13}C NMR.

3. Nile Red Assay[3]

This assay was employed to determine the critical micellar concentration (CMC) for the binders. A Nile red (2.5 mM) stock solution was made in EtOH. Solutions of Binder were prepared at a variety of concentrations starting from (300 μM) and less in disposable cuvettes. Samples of the stock solution were diluted by PBS to the required concentration in a 1 mL assay volume. Nile red (1 μL) was applied to each sample to give concentration of (2.5 μM). The fluorescence emission was measured using an excitation wavelength of 550 nm. Fluorescence intensity was recorded at 635 nm. This procedure was performed in triplicate.

We carried out this assay under different conditions for C_{16}-DAPMA in order to determine the impact of environment on self-assembly (Table S1). In buffered conditions (Tris) the CMC decreases from (67 ± 5) μM to (40 ± 1) μM in the presence of salt, whereas in unbuffered water the CMC is significantly higher on addition of salt, increasing from (37 ± 3) μM to (72 ± 5) μM. The decrease in CMC in buffered conditions suggests enhanced self-assembly, in agreement with observations from Bromfield *et al* for the effect of salt on a related system, in which salt screening of the micellar surface charges enhances assembly.[4] In unbuffered water, we suggest that pH changes may be significant – hence the difference. Interestingly, the binders were more soluble when the salt was added *after* dissolving the binders in pure solvent.

Table S1: CMCs [μM] for C_{16}-DAPMA in different solvent with and without the presence of sodium chloride (150 mM).

C_{16}-DAPMA	**Tris**	**Tris + NaCl**	**H_2O**	**H_2O + NaCl**
CMC [μM]	67 ± 5	40 ± 1	37 ± 3	72 ± 5

Table S2: CMCs [μM] for all Binders in Tris and water in the presence of salt. *measured with hot solutions.

CMC [μM]	**C_{16}-DAPMA**	**C_{16}-SPD**	**C_{16}-SPM**
Tris + NaCl	40 ± 1	51 ± 2	65 ± 20*
H_2O + NaCl	72 ± 5	52 ± 2	42 ± 6

* measured with hot solution owing to low solubility

To further probe the effect of salt on assembly, we monitored the other binders under the key conditions (Table S2). In Tris, C_{16}-DAPMA assembled most effectively, while C_{16}-SPM struggled to dissolve and had a higher CMC. This is in agreement with the higher charge of the C_{16}-SPM surface groups under these conditions leading to electrostatic repulsion and limiting assembly. In unbuffered water, the trend was inverted, with C_{16}-SPM assembling most effectively, presumably because the pH of the system could change under these conditions, limiting the degree of protonation of the amine units and assisting self-assembly of this larger amine.

4. Dynamic Light Scattering

The measurements were made of the backscattered light fluctuations at an angle of 173° and calculation of an autocorrelation function. The samples were measured at 25 °C, adjusted to the temperature for 1 minute prior to measurement. The autocorrelation functions were analysed using the DTS v5.1 software provided by Malvern. Measurements were done in triplicate with 10-15 runs per single measurement and the calculated mean values (based on intensity and volume distribution) were used. The samples were measured in 10 mM Tris

HCl buffer and in ultrapure water. The samples were measured after filtering through nylon filters (0.45µm) to remove all dust from them.

DLS data are presented in Figs. S1-S3 as volume distributions. The intensity distributions (not shown) also indicated the presence of a larger aggregate (ca. 100 nm) – however, larger aggregates give rise to much larger scattering intensities, and once this is corrected for, the larger aggregates observed in the intensity distribution become insignificant. The larger aggregates were had higher intensity for C_{16}-DAPMA and C_{16}-SPD than for C_{16}-SPM which might be expected as a result of their smaller hydrophilic groups in comparison to the lipophilic unit.

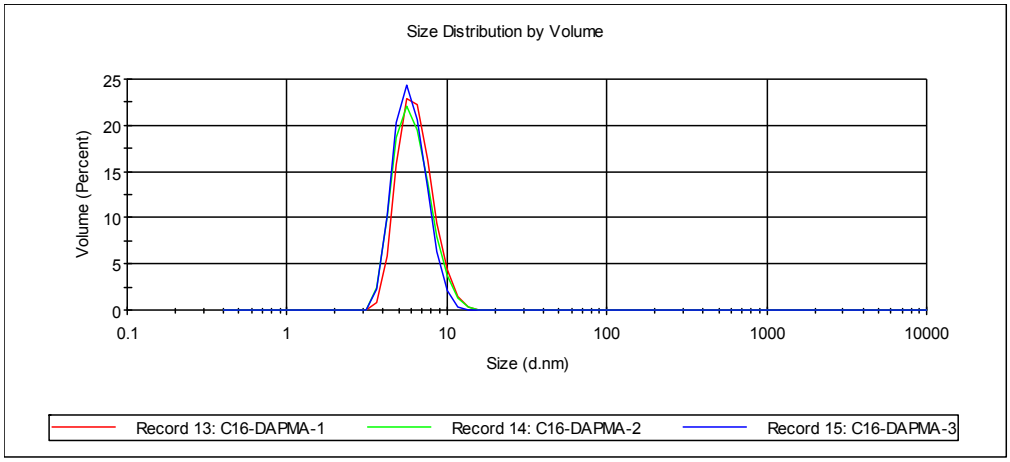

Figure S1. DLS of C_{16}-DAPMA showing size distribution by volume; one peak for each run.

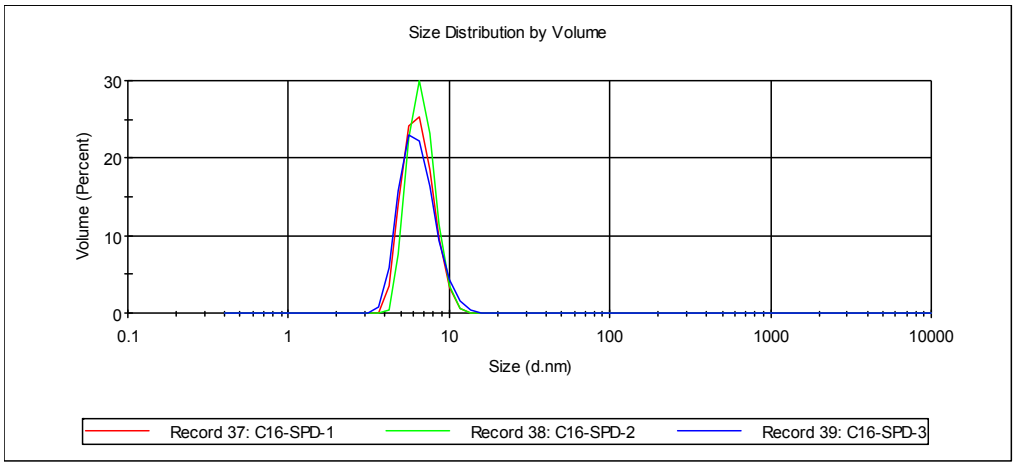

Figure S2. DLS of C_{16}-SPD showing size distribution by volume; one peak for each run.

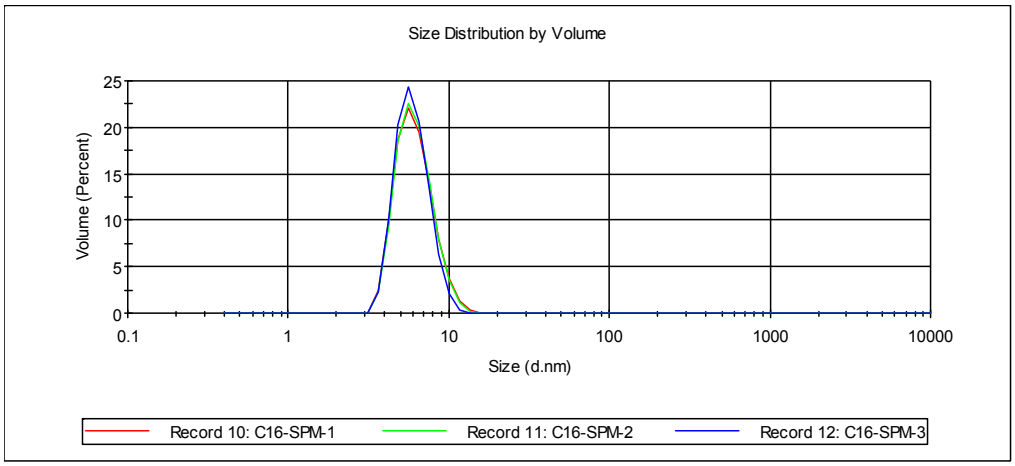

Figure S3. DLS of C_{16}-SPM showing size distribution by volume; one peak for each run.

Table S3. DLS data based on the volume contribution for compounds in the presence of either DNA (4 μM per base) or Heparin (27 μM per disaccharide repeat). The charge ratio +:- present in the cuvette was 0.1. The systems which are closer to forming charge neutral aggregates correspond with those systems which exhibit the best binding in the other assays.

		C_{16}-DAPMA (+2)	C_{16}-SPD (+2)	C_{16}-SPM (+3)
Diameter / nm	DNA	188 ± 13	198 ± 12	192 ± 45
	Heparin	137 ± 4	140 ± 50	305 ± 55
Zeta Potential	DNA	-24.6 ± 0.3	-21.1 ± 2.1	-11.2 ± 0.5
	Heparin	38.1 ± 1.0	9.8 ± 1.8	21.3 ± 4.2

5. Transmission Electron Microscopy Images

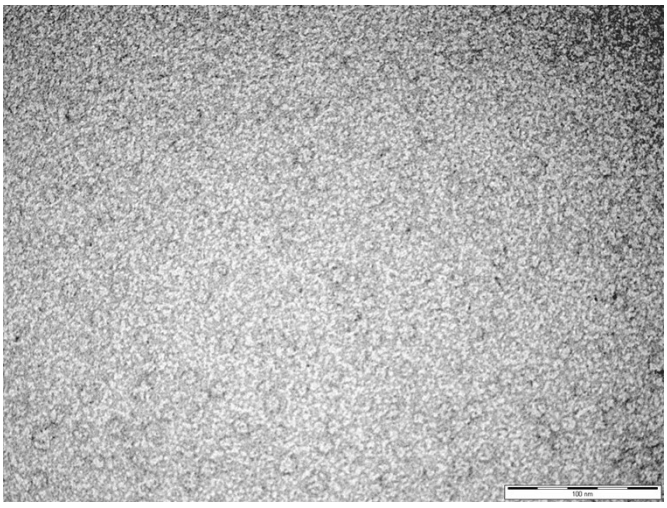

Figure S4. TEM image of C_{16}-DAPMA.

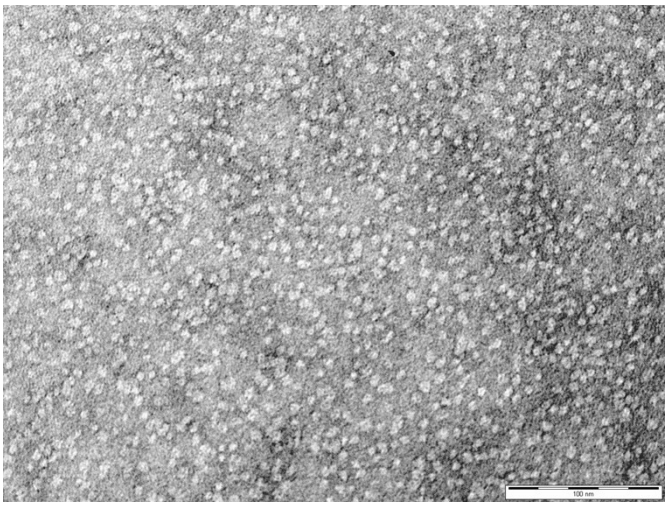

Figure S5. TEM image of C_{16}-SPD.

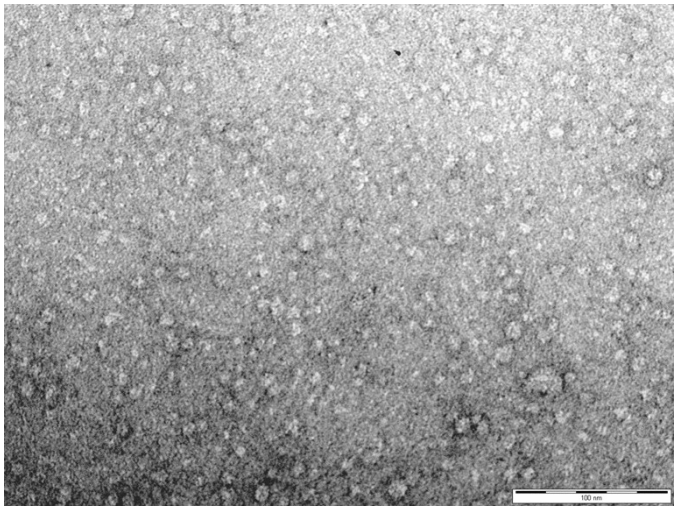

Figure S6. TEM image of C_{16}-SPM.

6. Mallard Blue (MalB) Assay for Heparin Binding[5]

MalB (25 μM) solution was incubated at 50 °C for 24 hours prior to use and was wrapped with foil to ensure that the dye was not exposed to direct light. 2 mL of MalB (25 μM), heparin (27 μM) and NaCl (150 mM) in Tris HCl (10 mM) was placed in a cuvette then titrated with binder stock solution to give a suitable charge ratio for the binder and heparin in the cuvette. Binder stock solution consisted of the original solution of MalB/Heparin/NaCl/Tris HCl stock solution, then a concentration of binder 2 was added so that, after 10 μL binder stock, the cuvette charge ratio (+ : -) is 0.1 . After each addition the mixture in the cuvette was stirred (with clean plastic pipette) to ensure total mixing and the absorbance was recorded at 615 nm against the baseline of the Tris HCl (10 mM). The

normalization of the absorbance was made between two solutions, the first one was MalB (25 μM) and NaCl (150 mM) in Tris HCl (10 mM) and the other contained MalB (25 μM), heparin (27 μM) and NaCl (150 mM) in Tris HCl (10 mM). This procedure was performed in triplicate.

7. Ethidium Bromide Assay for DNA Binding[6]

A solution of Calf Thymus DNA (8.0 μM) was prepared in SHE buffer (2 mM HEPES, 0.05 mM EDTA, 150 mM NaCl) at pH 7.5. Ethidium bromide was diluted with SHE Buffer to give a final concentration of 10.14 μM. Background ethidium bromide fluorescence was measured at 5.07 μM. The binder stock solution, at varying concentration depending on the charge of the binder, was prepared in a 50:50 solution of the ethidium bromide and DNA solutions to give a final EthBr concentration of 5.07 μM and DNA at 4.0 μM with respect to one DNA base (M_r 330 $gmol^{-1}$). Appropriate amounts of the binder solution were added to 2 ml of a stock solution containing EthBr (5.07 μM) and DNA (4.0 μM) to achieve the desired charge ratio (+ : -). The fluorescence was measured using an excitation wavelength of 540 nm. Fluorescence intensity was recorded at 595 nm. The fluorescence values were normalised to a solution containing only DNA (4.0 μM) and EthBr (5.07 μM). This procedure was performed in triplicate.

In order to estimate the CMC in the presence of polyanion – linear fitting of the first two regions of this graph was performed (Fig. S4) – it was assumed that on initial addition of binder, it is non-assembled and cannot efficiently displace EthBr, however, once a critical concentration is reached, assembly is initiated under these conditions (encouraged by the presence of DNA) and the displacement of EthBr becomes more significant. Based on this assumption, the point at which these lines intersect can be proposed as a critical aggregation concentration under these assay conditions. Similar analysis could be performed for all of the EthBr and MalB assays and the data presented in Table S3 extracted.

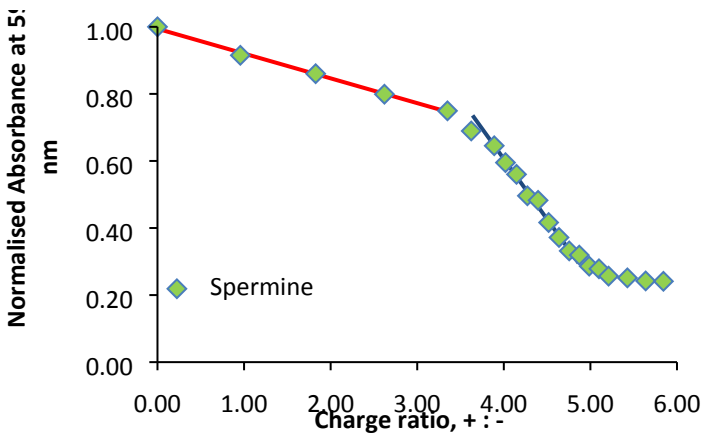

Figure S4. EthBr displacement assay data for C_{16}-SPM binding to DNA showing breakdown into two linear regions. The initial region (red) shows low-affinity binding to DNA prior to effective self-assembly of C_{16}-SPM, while the second region (blue) shows high-affinity binding to DNA once self-assembled multivalency has been switched on.

Table S4: CMCs from NileRed, MalB and EthBr assay.

CMC [μM]	**C_{16}-DAPMA**	**C_{16}-SPD**	**C_{16}-SPM**
Nile Red (Tris + NaCl)	40 ± 1	51 ± 2	65 ± 20*
MalB (Tris+NaCl+Hep+MalB)	12.7 ± 0.9	9.8 ± 0.9	8.9 ± 0.3
EthBr (SHE+ NaCl+DNA+EthBr)	8.2 ± 0.7	9.3 ± 0.3	4.8 ± 0.1

* measured with hot solution owing to low solubility

It is clear that in all cases, the apparent CMC value in the presence of polyanion is much lower than in its absence, and that anion binding encourages the self-assembly effect – in this way, self-assembled multivalency can be considered to enhance both binding *and* self-assembly, with the two effects reinforcing one another. It is also clear that the trends in apparent CMC match the observed trends in polyanion binding performance reported in the main paper, as such, we propose that those systems which bind best to the polyanions exhibit enhanced self-assembly as a result. Finally, it is evident that the two different polyanions induce markedly different effects on the apparent CMC – a clear difference between the

behaviour of heparin and DNA. Importantly, these apparent CMC values match those determined by ITC methods and described in the main part of the manuscript.

8. Isothermal Titration Calorimetry

Isothermal Titration Calorimetry (ITC) experiments were conducted using a Nano ITC Technology (TA Instruments, New Castle, DE, USA). Binding conditions were optimized for each SAMul ligand. The thermodynamic of micellization of all SAMul molecules was investigated in Tris HCl/150 mM NaCl buffered solutions. The same solution conditions were employed to obtain the thermodynamic parameters for heparin/SAMul ligands binding, while for DNA binding SHE/150 mM NaCl buffered solutions were used. In the binding assays, DNA and heparin initial concentration in the corresponding buffered solutions was 30 μM. All solutions and buffers used in the experiments were degassed for 30 min at room temperature under stirring at 350 rpm prior to experiment. Upon filling cell and syringe, stirring was turned and the each system was allowed to thermally equilibrate for 30 minutes. The enthalpy change caused by DNA/heparin dilution, measured under the same circumstances by titration buffer/NaCl solutions into the corresponding solutions, was found to be very small and therefore was neglected. Raw data curves were integrated with Microcal Origin Software, as described in the instrument manual. Statistics were performed on the thermodynamic parameters with a desired confidence interval of 95%. Each experiment was repeated in duplicate, and show excellent reproducibility.

Figure S5 shows ITC results obtained for the micellisation of C_{16}-DAPMA as an example.

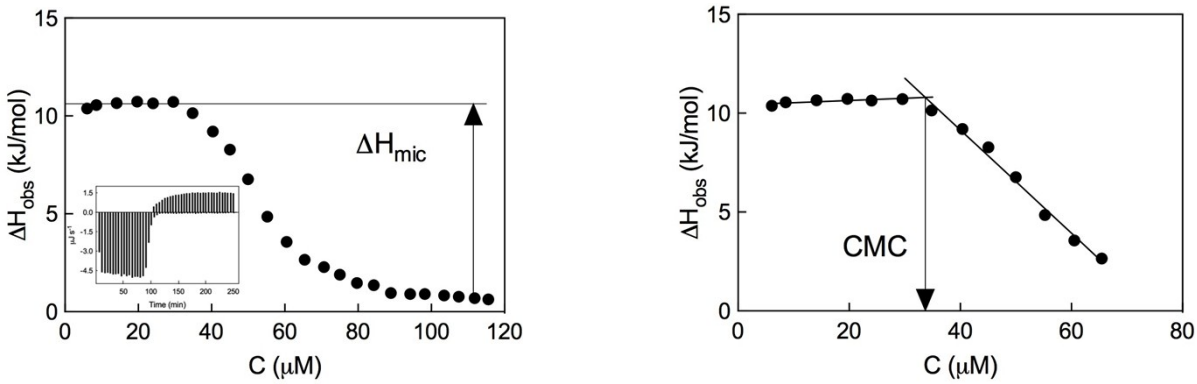

Figure S5. (Left) Calorimetric titration curve of C_{16}-DAPMA into a 150 mM NaCl solution at room temperature. ITC raw data are shown in the inset. (Right) Determination of C_{16}-DAPMA CMC from the calorimetric titration curve on the left.

Figures S6 and S7 illustrate the ITC results obtained for of C_{16}-DAPMA (Fig. S6) and C_{16}-SPM (Fig. S7) in the presence of 30 μM of DNA and heparin, respectively.

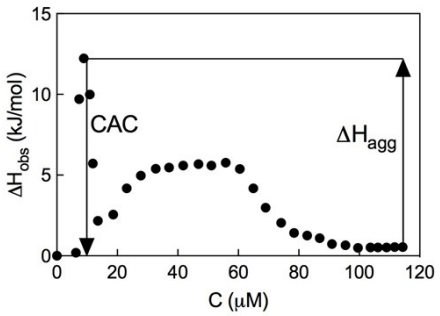

Figure S6. Calorimetric titration curve of C_{16}-DAPMA into a 30 μM DNA solution at 150 mM NaCl at room temperature.

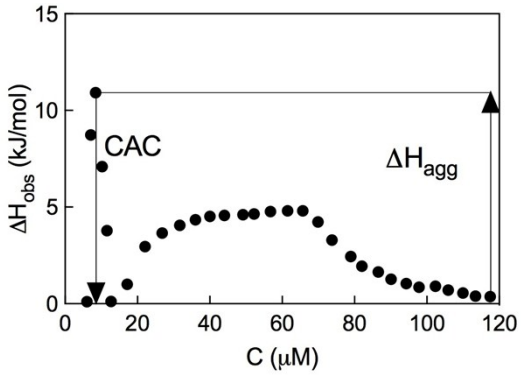

Figure S7. Calorimetric titration curve of C_{16}-SPM into a 30 μM heparin solution at 150 mM NaCl at room temperature.

9. Multiscale Modeling Methods

9.1 Multiscale Modeling of Self-Assembly Process

In this work, we resorted to our well-validated multiscale molecular modeling procedure[7-11] based on the systematic elimination of computationally expensive degrees of freedom while retaining implicitly their influence on the remaining degrees freedom in the mesoscopic model. Accordingly, using the information obtained from atomistic molecular dynamics simulation (MD), we parameterized the dissipative particle dynamics (DPD)[12] models that incorporate all essential physics/phenomena observed at the finer level. The outline of the general strategy of our multiscale modeling approach may be summarized as follows: i) explicit solvent atomistic MD calculations[13] were performed on C_{16}-DAPMA, C_{16}-SPD, and

C_{16}-SPM and their assembly; ii) coarse-grained DPD simulations were carried out at concentrations higher than the experimental CAC and the aggregates were characterized in terms of dimension and aggregation number; the mesoscale model parameters were calculated exploiting the conformational properties and energetic values obtained from MD simulation at point (i)[14] using an explicit solvent model in which each molecule was represented as single force centers (beads) and solvent was treated explicitly in the presence of ions and counterions. Langevin dynamics were then conducted using the DPD representation of the system; iii) the equilibrium configurations of the self-assembled systems obtained at point (ii) were mapped back to the corresponding atomistic MD models, and then new atomistic MD simulations were conducted to calculate binding energies between each micelle and DNA as well as the heparin molecule.

9.2 Atomistic Molecular Dynamics Simulation of the Amphiphilic Molecules and their Assembly

All atomistic simulations and data analysis were performed with the AMBER 14 suite of programs.[15] The models of the C_{16}-DAPMA, C_{16}-SPD, and C_{16}-SPM compounds were built and geometry-optimized using the Antechamber module of AMBER 14 and the GAFF force field.[16] The molecule structures were then solvated in a TIP3P[17] water box to generate a bulk system with a concentration lower than the corresponding experimental CAC value. Then, the required amount of Na^+ and Cl^- ions were added to neutralize the system and to mimic salt conditions, removing eventual overlapping water molecules. The solvated molecules were subjected to a combination of steepest descent/conjugate gradient minimization of the potential energy, during which all bad contacts were relieved. The relaxed systems were then gradually heated to 300 K in three intervals by running constant volume-constant temperature (NVT) MD simulation, allowing a 0.5 ns interval per 100 K. Subsequently, 10 ns MD simulations under isobaric-isothermal (NPT) conditions were conducted to fully equilibrate each solvated compound. The *SHAKE* algorithm[18] with a geometric tolerance of $5x10^{-4}$ Å was imposed on all covalent bonds involving hydrogen atoms. Temperature control was achieved using the Langevin[19] temperature equilibration scheme and an integration time step of 2 fs. At this point, these MD runs were followed by other 20 ns of NVT MD simulation. The particle mesh Ewald (PME) method[20] was used to treat the long-range electrostatics. Exploiting the morphological information obtained at the mesoscale level (*vide infra*), the corresponding atomistic models of C_{16}-DAPMA, C_{16}-SPD, and C_{16}-SPM micelles were built and placed in a cubic box filled with water molecules extending at least 20 Å from the solute

(Figure S8A). A suitable number of Na^+ and Cl^- ions was added to neutralize the system and to mimic ionic strength. The supramolecular assembly was relaxed according to the procedure described above (Figure S8B), followed by 100 ns of NVT MD (Figure S8C). All of the production molecular dynamics simulations were carried out working in our own CPU/GPU hybrid cluster.

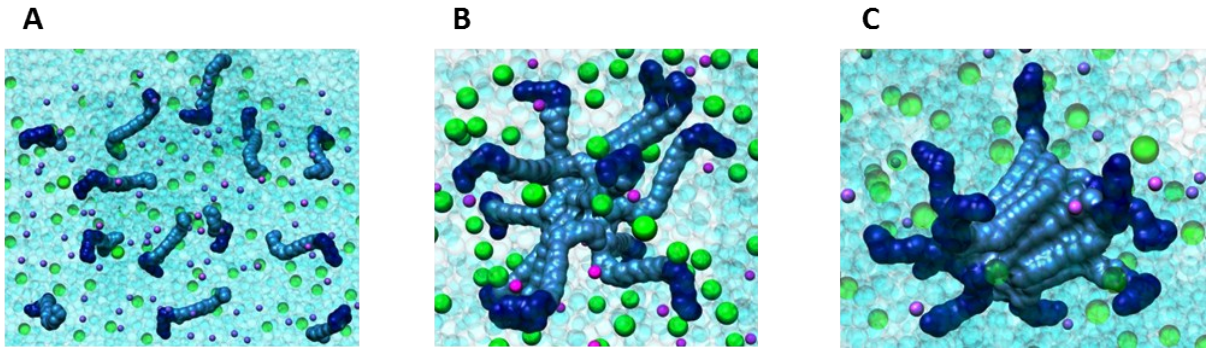

Figure S8. Atomistic simulations of C_{16}-SPM self-assembly process into spherical micelles. The panel represent the MD snapshots of the starting point (**A**, 0 ns), an intermediate state (**B**, 10 ns) and the final stage (**C**, 100 ns) of the assembly. The C_{16}- hydrophobic portion is shown as steel blue spheres whereas the SPM residues are portrayed as navy blue spheres. Water molecules are depicted as transparent light blue spheres whereas some Na^+ and Cl^- ions are shown as purple and green spheres, respectively.

9.3 DPD modeling of C_{16}-DAPMA, C_{16}-SPD, and C_{16}-SPM Self-Assembly

Comparing the appropriate MD and DPD pair-pair correlation functions, we determined the mesoscale topology of each compound in solution, according to a procedure validated by our group on other, related self-assembling compounds.[21-24] Accordingly**,** at a coarse-grained level we modelled the different ligands using amphiphilic chains made up of 5 bead types as shown in Figure S9: three different charged amine moieties N1, N2, and NM, one hydrophobic building block C, representing the alkyl chain, and one further bead type, L, featuring an amide group. Solvent molecules were simulated by single bead types W, and an appropriate number of counterions of a charge of ± 1 were added to preserve charge neutrality and to account for the ionic strength.

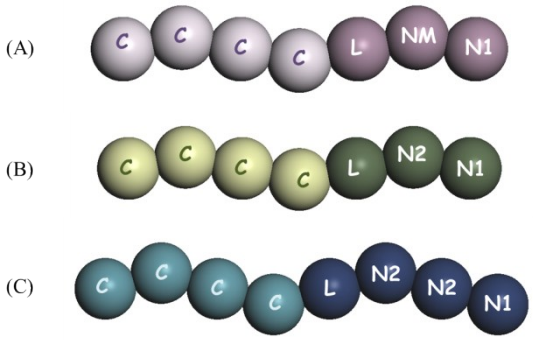

Figure S9. Schematic representation of the coarse-grained DPD models of C_{16}-DAPMA (**A**), C_{16}-SPD (**B**), and C_{16}-SPM (**C**).

All simulations were performed in 3D-periodic cubic boxes. The appropriate number of C_{16}-DAPMA, C_{16}-SPD, and C_{16}-SPM molecules was added to the simulation box in order to fit experimental concentrations. Intra- and intermolecular interactions between DPD particles are expressed by a conservative, soft-repulsive force, vanishing beyond a certain cutoff radius r_c, whose value sets the unit length in simulations. The intensity of this conservative force is defined by a pair-repulsive parameter a_{ij}, which accounts for the underlying chemistry of the system considered. In this work, we employed a well-validated strategy that correlates the interaction energies estimated from atomistic MD simulations to the mesoscale a_{ij} parameter values.[21-27] Following this computational recipe, the atomistic interaction energies between the components of the solvated C_{16}-DAPMA/ C_{16}-SPD/C_{16}-SPM systems were estimated using the Molecular Mechanics/Poisson Boltzmann Surface Area (MM/PBSA) methodology[28] (*vide infra*) as implemented in the Amber 14 package. Once obtained, the atomistic interaction energies were rescaled onto the corresponding mesoscale segments adapting the procedure described in detail in reference.[27] The self-repulsive interaction parameters for water were set equal to $a_{WW} = 25$ in agreement with the correct value of DPD density $\rho = 3$.[12] The maximum level of hydrophobic/hydrophilic repulsion was captured by setting the interaction parameter a_{ij} between the water bead W and the alkyl tail bead C as 80. The counterions were set to have the interaction parameters of water.[29] Once these parameters were assigned, all the remaining bead-bead interaction parameters for the DPD simulations were easily obtained, starting from the atomistic interaction energies values (Table S4).

Table S5. DPD bead-bead interaction parameters used in this work.

a_{ij}	*C*	*L*	*N1*	*N2*	*NM*	*W*
C	26					
L	48	29				
N1	74	33	39			
N2	72	34	37	38		
NM	77	36	38	39	41	
W	80	34	24	22	26	25

Unless otherwise stated, in all DPD studies the following reduced units were used: r_c is the unit of length, m is the mass of a DPD particle, and kT is the unit of energy. Simulations were carried out at a total particle density of $\rho = 3$ in a box of 40 r_c^3 with a time step of $\Delta t = 0.04$ and a simulation period of 1 x 10^5 steps or longer until stable morphology was observed. All mesoscale simulations were performed using Materials Studio v. 5.0 software.

9.4 Atomistic molecular dynamics simulations of C_{16}-DAPMA, C_{16}-SPD, and C_{16}-SPM micelles in complex with DNA and heparin

The model system of C_{16}-DAPMA, C_{16}-SPD, and C_{16}-SPM micelles described above was taken from an equilibrated configuration of the assembly, removing all water molecules and ions. The complex of DNA and heparin with C_{16}-DAPMA, C_{16}-SPD, and C_{16}-SPM micelle, was then achieved by adapting a consolidated procedure developed by our group.[5] Accordingly, it will be reported here briefly. To build the 3D models of the complexes, the biomolecule chain was initially placed close to each micelle periphery. The resulting molecular pair was subsequently energy minimized to yield a starting structure devoid of substantial van der Waals overlaps. Each complex was then solvated with an appropriate number of TIP3P[17] water molecules extending at least 20 Å from the solute. A suitable number of Na^+ and Cl^- counterions were added to neutralize the system and to mimic the salt conditions. Eventual overlapping water molecules were removed. Each complex molecular model was then subjected to a combination of steepest descent and conjugate gradient energy minimization steps (50000 cycles), in order to relax close atomic distances. The energy-minimized systems were further equilibrated by performing 10 ns MD simulations in the NPT ensemble using an integration step of 1fs. During equilibration, different energetic components as well as static and conformational properties were monitored, to ensure their

stabilization prior to production runs. MD production runs were performed on equilibrated systems again in the NPT ensemble with 1 fs time step (T = 300 K, P = 1 bar). The Langevin method for the control of temperature (with a damping coefficient of 5 ps^{-1}) and the Nose-Hoover Langevin piston method[30] for the control of pressure (using a piston period of 0.8 ps and a decay time of 0.4 ps) were employed for temperature and pressure control, respectively. Electrostatic interactions were computed by means of the PME algorithm.[16] Subsequently, the production MD trajectories of 100 ns were generated. For the calculation of the binding free energy between heparin and each compound, 10000 snapshots were saved during the MD data collection period described above, one snapshot per each 10 ps of MD simulation.
All of the production (MD) simulations were carried out using AMBER 14 platform by applying the *ff14SB* and the *gaff* force field[31] working in our own CPU/GPU hybrid cluster. All energetic analyses were performed by running the MM/PBSA script supplied with AMBER 14 on a single MD trajectory of each complex considered.

To estimate the free energy of binding ΔG_{bind} between DNA or heparin and each compound, we resorted to a well-established computational recipe[32] based on the MM/PBSA methodology.[28] Briefly, for a non-covalent association of two molecular entities A + B → AB, the free energy of binding involved in the process may be generally written as $\Delta G_{bind} = G_{AB} - G_A - G_B$. For any species on the right hand side of this equation, from basic thermodynamics we have $G_i = H_i - TS_i$, where H_i and S_i are the enthalpy and entropy of the i-th species, respectively and T is the absolute temperature. In view of this expression, ΔG_{bind} can then be written as: $\Delta G_{bind} = \Delta H_{bind} - T\Delta S_{bind}$. ΔH_{bind} is the variation in enthalpy upon association and, in the MM/PBSA framework of theory, can be calculated by summing the molecular mechanics energies (ΔE_{MM}) and the solvation free energy (ΔG_{solv}), i.e., $\Delta H_{bind} = \Delta E_{MM} + \Delta G_{solv}$. Finally, the estimation of the entropic contribution $- T\Delta S_{bind}$ is performed using normal mode analysis, which requires the computation of eigenvectors and eigenvalues via the diagonalization of the Hessian matrix.

We deconvoluted the enthalpic term of the *effective* free energy of binding into its main components for each individual *effective* (i.e., contributing actively to the binding) charged residues (RESC) of C_{16}-DAPMA, C_{16}-SPD, and C_{16}-SPM in complex with DNA and heparin. This allowed us to determine the relative contribution of electrostatic binding and dispersion interactions to the overall binding event, and hence determine the dominant factors

controlling the response of binding. Finally, the effective number of charges involved in binding, and the corresponding effective free energy of binding values (main text, Figure 5) were obtained performing a per residue binding free energy decomposition (PRBFED) exploiting the MD trajectory of each given heparin complex. This analysis was carried out using the MM/GBSA approach,[33] and was based on the same snapshots used in the binding free energy calculation.

10. References

1. I. S. Blagbrough and A. J. Geall, *Tetrahedron Lett.*, 1998, **39**, 439-442.

2. R. Andruszkiewicz, M. Radowski and Z. Czajgucki, *Synth. Commun.*, 2005, **35**, 1085-1094.

3. M. C. A. Stuart, J. C. van de Pas and J. B. F. N. Engberts, *J. Phys. Org. Chem.*, 2005, **18**, 929-934.

4. S. M. Bromfield, P. Posocco, C. W. Chan, M. Calderon, S. R. Guimond, J. E. Turnbull, S. Pricl and D. K. Smith, *Chem. Sci.*, 2014, **5**, 1484-1492.

5. S. M. Bromfield, P. Posocco, M. Fermeglia, S. Pricl, J. Rodríguez-López and D. K. Smith, *Chem. Commun.*, 2013, **49**, 4830-4832.

6. (*a*) B. F. Cain, B. C. Baguley and W. A. Denny, *J. Med. Chem.*, 1978, **21**, 658-668. (*b*) D. L. Boger, B. E. Fink, S. R. Brunette, W. C. Tse and M. P. Hedrick, *J. Am. Chem. Soc.*, 2001, **123**, 5878-5891.

7. S. M. Bromfield, A. Barnard, P. Posocco, M. Fermeglia, S. Pricl and D. K. Smith, *J. Am. Chem. Soc.*, 2013, **135**, 2911-2914.

8. P. Posocco, E. Laurini, V. Dal Col, D. Marson, K. Karatasos, M. Fermeglia and S. Pricl, *Curr. Med. Chem.*, 2012, **19**, 5062-5087.

9. X. Liu, J. Wu, M. Yammine, J. Zhou, P. Posocco, S. Viel, C. Liu, F. Ziarelli, M. Fermeglia, S. Pricl, G. Victorero, C. Nguyen, P. Erbacher, J. P. Behr and L Peng, *Bioconjugate Chem.*, 2011, **22**, 2461-2473.

10. S. P. Jones, N. P. Gabrielson, C. H. Wong, H. F. Chow, D. W. Pack, P. Posocco, M. Fermeglia, S. Pricl and D. K. Smith, *Mol. Pharmaceutics*, 2011, **8**, 416-429.

11. P. Posocco, S. Pricl, S. P. Jones, A. Barnard and D. K. Smith, *Chem. Sci.*, 2010, **1**, 393-404.

12. (*a*) R. D. Groot and P. B. Warren, *J. Chem. Phys.*, 1997, **107**, 4423-4435. (*b*) P. J. Hoogerbrugge and J. M. V. A. Koelman, *Europhys. Lett.*, 1992, **19**, 155-160.

13. (*a*) X. Liu, C. Liu, E. Laurini, P. Posocco, S. Pricl, F. Qu, P. Rocchi and L. Peng, *Mol. Pharmaceutics*, 2012, **9**, 470-481. (*b*) K. Karatasos, P. Paola, E. Laurini and S. Pricl, *Macromol Biosci.* 2012, **12**, 225-240.

14. P. Posocco, C. Gentilini, S. Bidoggia, A. Pace, P. Franchi, M. Lucarini, M. Fermeglia, S. Pricl and L. Pasquato, *ACS Nano*, 2012, **6**, 7243-7253.

15. D. A. Case, V. Babin, J. T. Berryman, R. M. Betz, Q. Cai, D. S. Cerutti, T. E. Cheatham, T. A. I. Darden, R. E. Duke, H. Gohlke, A. W. Goetz, S. Gusarov, N. Homeyer, P. Janowski, J. Kaus, I. Kolossváry, A. Kovalenko, T. S. Lee, S. LeGrand, T. Luchko, R. Luo, B. Madej, K. M. Merz, F. Paesani, D. R. Roe, A. Roitberg, C. Sagui, R. Salomon-Ferrer, G. Seabra, C. L. Simmerling, W. Smith, J. Swails, R. C. Walker, J. Wang, R. M. Wolf, X. Wu and P. A. Kollman, 2014, AMBER 14, University of California, San Francisco.

16. (*a*) J. Wang, R. M. Wolf, J. Caldwell, P. A. Kollman and D. A. Case, *J. Comput. Chem.*, 2004, **25**, 1157-1174. (*b*) J. Wang, P. A. Kollman and D. A. Case, *J. Mol. Graph. Model.*, 2006, **25**, 247-260.

17. W. L. Jorgensen, J. Chandrasekhar, J. D. Madura, R. W. Impey and M. L. Klein, *J. Chem. Phys*., 1983, **79**, 926-935.

18. J.-P. Ryckaert, G. Ciccotti and H. J. C. Berendsen, *J. Comput. Phys.*, 1977, **23**, 327-341.

19. R. J. Loncharich, B. R. Brooks and R. W. Pastor, *Biopolymers*, 1992, **32**, 523-535.

20. A. Toukmaji, C. Sagui, J. Board and T. Darden, *J. Chem. Phys.*, 2000, **113**, 10913-10927.

21. T. Wei, C. Chen, J. Liu, C. Liu, P. Posocco, X. Liu, Q. Cheng, S. Huo, Z. Liang, M. Fermeglia, S. Pricl, X.-J. Liang, P. Rocchi and L. Peng, *Proc. Natl. Acad. Sci. USA*, 2015, **112**, 2978–2983.

22. X. Liu, J. Zhou, T. Yu, C. Chen, Q. Cheng, K. Sengupta, Y. Huang, H. Li, C. Liu, Y. Wang, P. Posocco, M. Wang, Q. Cui, S. Giorgio, M. Fermeglia, F. Qu, S. Pricl, Y. Shi, Z. Liang, P. Rocchi, J. J. Rossi and L. Peng, *Angew. Chem. Int. Ed.*, 2014, **53**, 11822-11827.

23. A. Barnard, P. Posocco, M. Fermeglia, A. Tschiche, M. Calderon, S. Pricl and D. K. Smith, *Org. Biomol. Chem.* 2014, **12**, 446-455.

24. S. M. Bromfield, P. Posocco, M. Fermeglia, J. Tolosa, A. Herreros-López, S. Pricl, J. Rodríguez-López and D. K. Smith, *Chem. Eur. J.*, 2014, **20**, 9666-9674.

25. D. J. Welsh, P. Posocco, S. Pricl and D. K. Smith, *Org. Biomol. Chem.*, 2013, **11**, 3177-3186.

26. S. Kala, A. S. Mak, X. Liu, P. Posocco, S. Pricl, L. Peng and A. S. Wong, *J. Med. Chem.*, 2014, **57**, 2634-2642;

27. G. Scocchi, P. Posocco, M. Fermeglia and S. Pricl, *J. Phys. Chem. B*, 2007, **111**, 2143-2151.

28. V. Tsui and D. A. Case, *Biopolymers*, 2000, **56**, 275-291.

29. X. Fan, N. Phan-Thien, S. Chen, X. Wu and T. Y. Ng, *Phys. Fluids*, 2006, **18**, 63102-63110.

30. S. E. Feller, Y. Zhang, R. W. Pastor and B. R. Brooks, *J. Chem. Phys*., 1995, **103**, 4613-4621.

31. Y. Duan, C. Wu, S. Chowdhury, M. C. Lee, G. M. Xiong, W. Zhang, R. Yang, P. Cieplak, R. Luo, T. Lee, J. Caldwell, J. Wang and P. Kollman, *J. Comput. Chem.*, 2003, **24**, 1999–2012.

32. J. Srinivasan, T. E. Cheatham, P. Cieplak, P. A. Kollman and D. A. Case, *J. Am. Chem. Soc.*, 1998, **120**, 9401-9409.

33. I. Massova and P. A. Kollman, *Perspect. Drug Discovery Des.*, 2000, **18**, 113-135.